

# Photocatalytic rate dependence on light absorption properties of different TiO<sub>2</sub> specimens

Paola Calza, Marco Minella, Luca Demarchis, Fabrizio Sordello, Claudio Minero\*

Università di Torino, Dipartimento di Chimica, Via Giuria 5 - 10125 Torino, Italy

\* Corresponding author: [claudio.minero@unito.it](mailto:claudio.minero@unito.it)

## Abstract

The light absorption and scattering play a prominent and often underrated role in the overall photocatalytic process and heavily affect the rate. This is particularly important for the choice of the catalyst in addition to other chemical and physical parameters usually considered for their catalytic role. Here we propose an approximated but easy-to-apply method to evaluate the light harvested by the photocatalyst slurry and its scattering/absorption coefficients, which does not require the use of complex spectrophotometric tools and the complicated radiative transport equation. The optical properties are obtained with the lamp and in the experimental setup employed in the photocatalytic batch tests. Among the four TiO<sub>2</sub> specimens considered, we characterized Evonik P25 and Hombikat UV100. The obtained scattering and absorption coefficients helped in rationalizing the experimental results on the degradation of formic acid at low concentration. From the rate dependence on the catalyst concentration, this approach allowed further understanding of the role of catalyst-specific properties affecting the overall catalytic performance. This approach is proposed as a starting point for fixing conditions to compare different photocatalysts.

## Keywords

Photocatalysis, TiO<sub>2</sub> specimens, kinetic analysis, scattering, absorption coefficient, formic acid.

## 26      **1. Introduction**

27      In the last decades many reports demonstrated that heterogeneous photocatalysis has  
28 unrivalled ability to abate persistent pollutants often until complete mineralization.[1-5]  
29 Nevertheless, commercial applications are still limited, because of the low efficiency in terms  
30 of low quantum yield and of the scarce ability of the most active photocatalysts to absorb  
31 solar light, increasing the costs and the requirement for water-treatment plants. [6]

32      The fundamentals of semiconductor photocatalysis are now well understood, and there is a  
33 general consensus that the photocatalytic process starts with the absorption of a photon (with  
34 energy  $h\nu$ ) from a semiconductor characterized by an energy gap  $E_g$  lower than the photon  
35 energy ( $h\nu \geq E_g$ ). This photoexcitation causes a change of the redox properties of the  
36 semiconductor surface, allowing charge transfer reactions through the semiconductor/solution  
37 interface. [7] The net result is the oxidation of the dissolved contaminants and the reduction of  
38 the electron acceptor - usually molecular oxygen and/or a reducible adsorbed substrate [8] -  
39 catalyzed by the irradiated semiconductor. [9, 10] Besides this apparent simplicity, the overall  
40 photocatalytic rate is the result of the complex interplay among many elementary reactions,  
41 whose relative importance is a complicated, and usually not reported function of the  
42 experimental setup and type of catalyst. An exhaustive mathematical treatment of the  
43 photocatalytic process results very complex and is still object of debate.

44      Several treatments to describe the photocatalytic rate have been proposed. One of the first  
45 and most successful models was the Langmuir-Hinshelwood (L-H) [7, 11, 12], which  
46 describes the degradative process in conditions of substrate adsorption at the catalysts surface.  
47 *Per se* the L-H treatment would be correct if the surface concentrations of reactive species,  
48 namely free or trapped electrons and holes, were fixed and constant, which is usually not the  
49 case. In general, these concentrations are function of the incident photon flux and the  
50 substrate nature and concentration. Conversely, the adsorption constants derived from the L-H  
51 model decrease with increasing light intensity, while the rate constant increases. [13]  
52 Therefore, L-H kinetic model cannot describe the overall rate, as demonstrate by Emeline and  
53 co-workers [14] and by Minero and Vione. [15] Despite the large agreement on the  
54 inadequacy of L-H model to interpret photocatalytic kinetic data, [7] it is largely diffuse the  
55 habit to correlate uncritically the Langmuir adsorption coefficients of the studied substrate  
56 with the related kinetic data forgetting that: *i*) the literature demonstrated the inadequacy of  
57 this model [16]; *ii*) the best isotherm describing the adsorption of a molecules on the surface  
58 of the most diffused photocatalysts is the Freundlich isotherm [17] and not the Langmuir one,  
59 although the last is useful for simple modelling. In 2007, Salvador and co-workers [18] -  
60 based on the model of reference [15] - developed the “Direct-Indirect” (D-I) kinetic model,  
61 assuming two different kinds of charge transfer to solution species, namely adiabatic and  
62 inelastic. The model was able to fit different sets of experimental data better than the L-H

63 model, [19] but still unsatisfactory, as in 2011 Rios et al. [20] stressed again the importance of  
64 back-reactions in the photocatalytic process, previously and largely supported by Minero and  
65 co-workers [11, 19, 21].

66 All these models highlights the importance of the chemical phenomena involved in the  
67 photocatalytic process, like adsorption, back-reactions, charge transfer dynamic and  
68 recombination. However, the light harvesting plays an equally important role in determining  
69 the rate, [15] as highlighted in the recent review by Egerton. [22] The optical properties of the  
70 semiconductor slurry are strongly related even with the state of agglomeration of the primary  
71 particles that dramatically influences the overall extinction properties (scattering and  
72 absorption) and ultimately the kinetics of the photocatalytic process. [22, 23] As a  
73 consequence, the particle dispersion determines the photocatalytic activity, owing to changes  
74 in slurry optical features and, therefore, suitable control experiments should be designed. [22]  
75 The importance of light absorption by the photocatalyst in the overall photocatalytic process  
76 has been evidenced by the impressive research efforts spent in the 3D structuration of  
77 photocatalysts to improve their performance. [24] The fact that semiconductor photonic  
78 crystals performed better compared with their nanoparticle homologues witnesses that light  
79 absorption and efficient light use by the photocatalyst allow significant room for the  
80 improvement of the performance. [25, 26]

81 This work focuses on effects of optical properties of some titanium dioxide specimens and  
82 on the evaluation of their role on the photocatalytic efficiency. We propose a simple  
83 experimental approach to estimate the optical parameters of slurries in the same apparatus that  
84 can be used to carry out the photocatalytic experiments. This procedure was applied to two  
85 different commercial TiO<sub>2</sub> specimens (Evonik P25 and Hombikat UV100). Furthermore, the  
86 relationship between the optical parameters and the kinetics of the photocatalytic process was  
87 assessed by monitoring formic acid transformation in the presence of the same TiO<sub>2</sub>  
88 photocatalysts at different loadings.

## 89 **2. Theoretical background**

90 Among many possible kinetic models, the quadratic kinetic model [15] gives a rate  
91 expression that is able to correctly predict the dependence on incident light intensity, initial  
92 substrate concentration and catalyst loading. This model was extensively validated [27], and  
93 has the advantage of having only one kinetic parameter, thus only one degree of freedom, that  
94 can help to avoid overfitting. [28] To determine and measure the influence played by the  
95 optical parameters of titanium dioxide suspensions on their photocatalytic efficiency we  
96 started from the expression of quantum yield  $\eta$  in the case of a photocatalytic process  
97 characterized by current doubling (see paragraph 4.2) [15]:

98 
$$\eta = -\frac{y}{2} + \sqrt{\frac{y}{2}\left(\frac{y}{2} + 2\right)}$$
 (1)

99 where the dimensionless master variable  $y = k_0 \cdot C_{Red1} \cdot C_{Ox2} \cdot \square_v^{-1}$ , in which  $k_0$  is a cumulative  
 100 kinetic constant (*vide infra*),  $C_{Red1}$  and  $C_{Ox2}$  are the molar concentrations of the substrate and  
 101 the oxidant in the system as a whole (semiconductor surface + water bulk, mol L<sup>-1</sup>) and  $\square_v$  is  
 102 the volumetric rate of radiation absorption (mol L<sup>-1</sup> s<sup>-1</sup>). Eq.(1) is a simplification of a more  
 103 general one, in which a second dimensionless variable  $\zeta$ , expressing the net fraction of light-  
 104 generated charge carriers that reach the surface, was present. In the model here adopted  $\zeta=1$ .  
 105 In the case of larger particles where resistance to charge carriers transfer to the surface could  
 106 be present, or when absorbed light is large,  $0 < \zeta < 1$ . This would change only the relative scalar  
 107 value of effective light absorbed.

108 In the limit of low quantum yield,  $\frac{y}{2} \ll 2$ , eq. (1) can be approximated to:

109 
$$\eta = -\frac{y}{2} + \sqrt{y}$$
 (2)

110 This holds true when: *i*)  $k_0$  is small, i.e. the photocatalytic process is hindered because of  
 111 large recombination and/or sluggish charge transfer at the surface; *ii*)  $C_{Red1}$  and/or  $C_{Ox2}$  are  
 112 small, thus favouring recombination over charge transfer; *iii*)  $\phi_v$  is large compared with  
 113  $k_0 \cdot C_{Red1} \cdot C_{Ox2}$ , which means that the recombination processes (*second* order with respect to the  
 114 charge carrier concentrations) overcome the charge transfer kinetics (*first* order with respect  
 115 to the charge carrier concentrations).

116 The rate of the photocatalytic process is given by definition as the product of quantum  
 117 yield and volumetric rate of absorption. Then

118 
$$\frac{rate}{C_{cat}} = -\frac{k'}{2} + \sqrt{\frac{k' \phi_v}{C_{cat}}}$$
 (3)

119 in which  $k' \cdot C_{cat} = k_0 \cdot C_{Red1} \cdot C_{Ox2}$ . In a one-dimensional photocatalytic reactor, like that used in  
 120 batch experiments where a container is illuminated from the top, the light intensity is a  
 121 function of the optical depth  $z$ , and, consequently, the volumetric rate of absorption  $\square_v(z)$  can  
 122 be expressed as  $\square_v(z) = \kappa(\lambda) \cdot I(z) \cdot 10^3$ , where  $\kappa(\lambda)$  represent the wavelength dependent  
 123 absorption coefficient (cm<sup>-1</sup>) and  $I(z)$  is the radiation intensity at the depth  $z$  inside the  
 124 solution in mol s<sup>-1</sup> cm<sup>-2</sup>. The observed rate is the integral of eq. (3) over the overall optical  
 125 depth  $b$ :

126 
$$\frac{rate_{obs}}{C_{cat}} = -\frac{k'}{2} + \frac{1}{b} \int_0^b \sqrt{\frac{k' \phi_v(z)}{C_{cat}}} dz$$
 (4)

127 Introducing the expression of  $\square_v(z)$  in eq. (4), and considering  $\kappa(\lambda) = 10^{-3} \ln(10) \cdot \varepsilon_{abs}(\lambda) \cdot C_{cat}$   
 128 (where  $\varepsilon_{abs}$  is the specific absorption coefficient in cm<sup>2</sup> g<sup>-1</sup>), one obtains eq. (5):

129 
$$\frac{rate_{obs}}{C_{cat}} = -\frac{k'}{2} + \sqrt{\ln(10) I_0 k' \varepsilon_{abs}(\lambda) \chi} \quad (5)$$

130 in which  $I_0$  is the incident radiation intensity at the top of the slurry expressed in mol s<sup>-1</sup> cm<sup>-2</sup>  
 131 and  $\chi$  is the dimensionless average square root of normalized absorbed light in the reactor  
 132 expressed as:

133 
$$\chi = \frac{1}{b} \int_0^b \sqrt{\frac{I(z)}{I_0}} dz \quad (6)$$

134 It is often not recognized that the rate expressed in eq. (5) provides a saturative dependence  
 135 on the substrate concentration. Almost the same behaviour is provided by the L-H equation,  
 136 but from an erroneous starting-point. [16] The kinetic relationship (5) has general  
 137 applicability, independently on the optical and morphological properties of particles, provided  
 138 that the slurry is sufficiently stable regarding sedimentation. The application of Eq.(5) needs  
 139 that the hypotheses under which it was derived are fulfilled, namely that: 1)  $y \ll 4$  (that is low  
 140 quantum yield regime). For quantum yield < 0.3-0.4 the approximated equation is always  
 141 valid. In the case that  $\zeta$  (see above) were < 1, this would proportionally reduce the maximum  
 142 quantum yield for which the model is applicable; 2) the original model does not take into  
 143 account the back reactions, which could be present with some substrates. This is not the case  
 144 for formic acid here used as substrate.

145 The intensity of the light as a function of the optical depth can be approximated with the  
 146 Kubelka–Munk (K-M) equation: [15]

147 
$$I(z) = \frac{v I_0}{u \sinh(v\sigma z) + v \cosh(v\sigma z)}, \text{ with } u = 1 + \frac{\kappa(\lambda)}{\sigma(\lambda)}, \text{ and with } v = \sqrt{u^2 - 1} \quad (7)$$

148 where the parameters  $\sigma(\lambda)$  and  $\kappa(\lambda)$  represent the wavelength dependent scattering and  
 149 absorption coefficients in cm<sup>-1</sup>. Eq. (7) reduces to the Lambert–Beer law for  $\sigma \rightarrow 0$ :

150 
$$I(z) = I_0 e^{-\kappa z} \quad (8)$$

151 The K-M equation explicitly gives the transmittance as a function of the optical path  $z$  using  
 152 scattering and absorption optical constants. It will be used to obtain these parameters from  
 153 experimental transmittance. Rigorously, Eq. (7) could only be applied when monochromatic  
 154 light is employed, or when the emission spectral range is sufficiently narrow that the  
 155 variations of the optical constants are negligible compared with the uncertainty of the adopted  
 156 technique. The approximation involved in K-M equation and its accuracy was studied using  
 157 the numerical solution of the integro-differential radiative transfer equation (RTE) for the  
 158 sparse distribution of spherical scatterers. Except for low optical thickness, the relative errors  
 159 are under few percent.[29] The numerical solution of RTE was used in reactor modelling and  
 160 for the evaluation of absorbed light [30, 31]. The use of a more complex tool like the

161 numerical solution of RTE to fit experimental data is obviously possible although requiring  
162 skills not available in all laboratories. The comparison with optical parameters obtained using  
163 K-M and the reported values obtained through the RTE solution is discussed later.

164 Here the integration along the irradiated slurry depth according to Eq.(6) was performed  
165 numerically on experimental data. An explanatory scheme of the adopted procedure to  
166 evaluate the optical properties of the investigated photocatalyst is reported in Figure 1-SM of  
167 the Supplementary Material, hereafter SM.

### 168 **3. Experimental**

#### 169 *3.1. Reagents and materials*

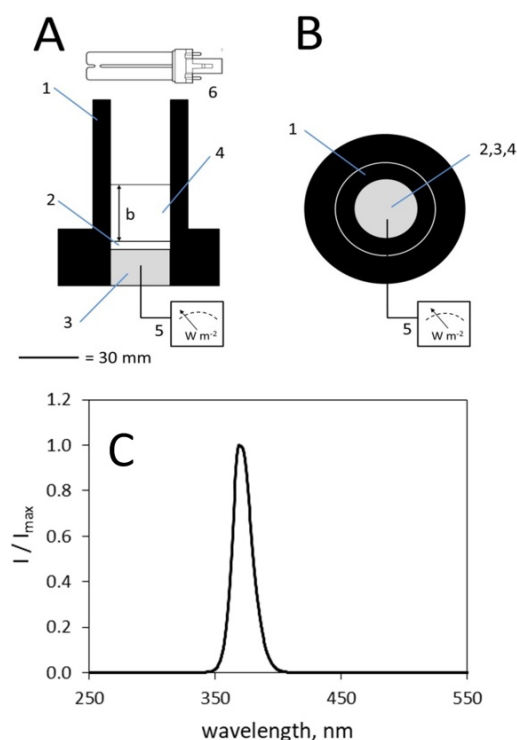
170 Formic acid (99%) was purchased from Riedel-de Haën, hydrochloric acid (37%) from  
171 Carlo Erba, potassium hydroxide (>99%) from Sigma-Aldrich. In this work four different  
172 types of commercial titanium dioxide were used: Evonik P25 (BET area ca 50 m<sup>2</sup>g<sup>-1</sup>, 80%  
173 anatase/20% rutile), Hombikat UV100 (BET area ca 348 m<sup>2</sup>g<sup>-1</sup>, 100% anatase), Merck TiO<sub>2</sub>  
174 (BET area ca 10 m<sup>2</sup>g<sup>-1</sup>, 100% anatase) and Wackherr TiO<sub>2</sub> (BET area ca 8.5 m<sup>2</sup>g<sup>-1</sup>, 100%  
175 anatase). The water used in all the experiments was of Milli-Q<sup>®</sup> quality. Titanium dioxide  
176 water suspensions were prepared by sonication with a 205W Branson 2200 sonicator for 15  
177 minutes.

#### 178 *3.2. Determination of optical properties*

179 The optical properties of each titanium dioxide specimen were determined through the  
180 evaluation of the  $\chi$  parameter through the measure of the transmittance as a function of the  
181 concentration of the semiconductor suspensions, recording the intensity of the light  
182 transmitted as a function of the optical path  $b$ .

183 For an accurate measurement of the transmission and of the  $\chi$  parameter, a custom-built  
184 cylindrical cell in black HDPE was used. This cell was fitted with an optical glass disk in the  
185 bottom (transmittance at 365 nm  $\approx$  100%, width = 5 mm), which allows the transmission of  
186 light and acts as support for TiO<sub>2</sub> suspensions. The UV probe with cosine correction working  
187 in the range 290-400 nm is housed immediately below the glass disk. The transmitted light  
188 was recorded using a CO.FO.ME.GRA (Milan, Italy) Solarbox Multimeter connected with the  
189 probe. A schematic representation of the device is reported in Figure 1 A, B. Data for the  
190 evaluation of the  $\chi$  parameter were obtained in a very short timescale (i.e. less than a minute),  
191 by measuring the transmission of few aliquots with fixed volume at a given  $C_{\text{cat}}$ . The  
192 numerous transmittance measures for optical parameter evaluation required longer time to be  
193 carried out (in the order of tens of minutes). These measurements at different optical depths  $b$

194 were carried out adding stepwise 0.5 mL of suspensions with diverse concentrations of TiO<sub>2</sub>.  
 195 In this temporal range the only titania specimens with sufficient stability were Evonik P25  
 196 and Hombikat UV100. The value of  $b$  was calculated from the known diameter of the cell.  
 197 The maximum  $b$  was limited to 12 mm, a value much lower than the height of the cell (70 mm  
 198 from the top of glass), to avoid cosine error from the illuminating source. The UV source was  
 199 a 9 W Philips PL-S lamp with an emission maximum at 360 nm (the normalized emission  
 200 spectrum of the lamp is reported in Figure 1C). It was positioned horizontally with respect to  
 201 the cell as evidenced on Figure 1A (not in scale).



202

203 **Figure 1. System used for the determination of the optical properties of TiO<sub>2</sub> suspensions. (A)**  
 204 **Transversal section; (B) view from above and (C) emission spectrum of the Philips PL-S 9W BLB lamp**  
 205 **normalized for the emission maximum. 1) HDPE walls; 2) optical glass disk; 3) UV probe; 4) TiO<sub>2</sub>**  
 206 **suspension with depth  $b$ ; 5) irradiance meter; 6) UV source.**

207

### 3.3. Irradiation experiments

208

209

210

211

212

213

Samples containing TiO<sub>2</sub> 0.1-1.0 g L<sup>-1</sup> and formic acid 0.2-1.0 mM were put into cylindrical Pyrex glass cells (4.0 cm diameter, 2.5 cm height). The UV source was the same used for the measurement of the optical properties. To ensure a controlled illumination distribution in the system, Pyrex cells were put into a home-made black HDPE container with the same size and geometry of the one described above for the optical measurements. Experiments were carried out in the presence of magnetic stirring. Samples were held for

214 several hours in the dark to reach the absorption equilibrium of formic acid on the catalyst  
215 surface before the start of the irradiation.

216 The photon irradiance at the top of the cells was  $20.3 \text{ W m}^{-2}$  in the 290-400 nm range,  
217 corresponding to  $6.1 \times 10^{-9} \text{ mol s}^{-1} \text{ cm}^{-2}$  considering 365 nm as the average wavelength of the  
218 photons emitted by the lamp.

219 After irradiation, samples were brought to pH 2 with hydrochloric acid to protonate formic  
220 acid and remove adsorbed molecules from the catalyst surface. After acidification,  
221 suspensions were filtered through  $0.45 \text{ }\mu\text{m}$  membranes (PTFE, Millipore), the pH was re-  
222 established with potassium hydroxide, and then analysed. The profiles of photocatalytic  
223 degradation of HCOOH were well described with first order kinetic equation  
224  $[F]_t = [F]_0 \exp(-k_{obs}t)$  where  $[F]_t$  is the formic acid concentration at time  $t$ ,  $[F]_0$  the initial  
225 concentration and  $k_{obs}$  the observed pseudo-first-order degradation rate constant. The initial  
226 degradation rate of formic acid was calculated as  $k_{obs}[F]_0$ .

### 227 3.4. Analytical determinations

228 The analysis of formate was carried out by means of ion chromatography with a Dionex  
229 DX 500 instrument equipped with an ED40 conductivity detector, a LC30 chromatography  
230 oven, a GP40 pump, an AS9-HC ion exchange column (250 mm x 4 mm i.d.), an ION PAC  
231 AG9-HC pre-column and an ASRS-ULTRA 4 mm suppressor. Formic acid was eluted with  
232 80/20 mixture of  $\text{K}_2\text{CO}_3$  9 mM/Milli-Q water with a flow rate of  $0.9 \text{ mL min}^{-1}$  and with an  
233 SRS current of 100 mA. Under these conditions, the retention time for formic acid was 4.95  
234 min.

## 235 4. Results and discussion

### 236 4.1. Optical properties of $\text{TiO}_2$ suspensions

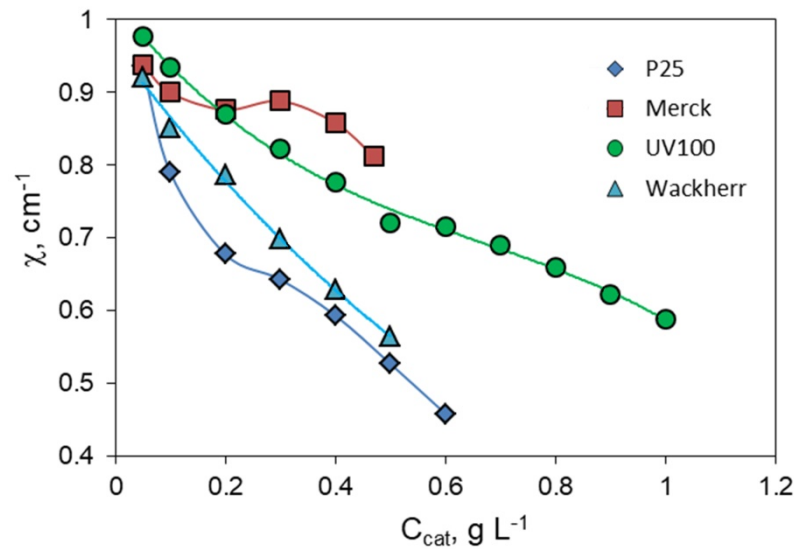
237 Figure 2 shows the value of  $\chi$  for the four different commercial  $\text{TiO}_2$  investigated as a  
238 function of the concentration of the photocatalyst. The  $\chi$  values were obtained by integrating  
239 the transmitted light intensity as a function of the optical path  $b$ , according with the definition  
240 of the parameter  $\chi$  in the eq. (6), up to a maximum  $b_{max} = 12 \text{ mm}$ .

241  $\chi$  decreases with the increment of  $C_{cat}$  for each catalyst. This is in agreement with the  
242 definition of  $\chi$ , as an increase in the semiconductors concentration leads to an enhanced  
243 intensity of light scattering and absorption, decreasing the average rate of absorption when  
244 considering the whole reactor. As the rate normalized for  $C_{cat}$  depends linearly on  $\chi$  (eq. 5),  
245 catalysts with more negative slope in Figure 2 are more subject to the so called *shielding*  
246 *effect* which is often invoked to explain the bell-shaped profile of the photocatalytic rate of a



247 process as a function of the catalyst loading of the slurry, [15, 32] also for organic  
248 photocatalysts. [33] With larger negative slopes, at the same  $C_{cat}$ , the strong extinction  
249 (scattering + absorption) in the very first layers of the irradiated slurry hinders photons to  
250 reach the bottom of the reactor decreasing the observed rate, which is averaged on the whole  
251 volume of the reactor.

252  $\text{TiO}_2$  Evonik P25 is characterized by the lowest values of  $\chi$ . This happens because P25 is  
253 characterized by a high intensity of scattering of the incident light compared with the other  
254  $\text{TiO}_2$  specimens (see also later for a discussion). [34]



255

256 **Figure 2. Values of the parameter  $\chi$  computed through Eq. (6) for different specimens of commercial**  
257  **$\text{TiO}_2$  at different catalyst concentrations.**

258 According to the eq. (5), a catalyst at a given  $C_{cat}$  with a high  $\chi$  could provide a degradation  
259 rate higher than that for a semiconductor with lower  $\chi$  values. This relationship is useful to  
260 compare the photocatalytic efficiency among different kinds of materials, and might allow the  
261 development of new types of catalysts with high efficiency by monitoring their optical  
262 properties.

263 The dependence of transmitted light intensity both on  $b$  value and catalyst concentration  
264 was carefully studied on Evonik P25 suspensions with loadings from 0.05 to 0.6 g L<sup>-1</sup>, and  
265 from 0.05 to 1.0 g L<sup>-1</sup> for Hombikat UV100. The different loading ranges were chosen  
266 because the larger extinction of P25 suspensions hinders the accurate determination of the  
267 light transmitted for larger loadings, even for short optical depths. The raw data are reported  
268 in Figure 2-SM. Each observed dependence on  $b$  values at fixed  $C_{cat}$  are well described by the  
269 Lambert-Beer law (where attenuation is due to the extinction coefficient) or alternatively by  
270 eq. (7) (see later), with the exception of the data at very low optical depth, especially with  
271 larger catalyst loadings. In these conditions the measured extinction is lower than the

272 predicted one, as a consequence of possible interfering optical phenomena, like the formation  
 273 of a convex meniscus acting as a lens, which converges the light onto the centre of the probe  
 274 body. This effect should be more important at low  $b$  and at large  $C_{cat}$  and could not be  
 275 completely compensated by the adopted cosine corrector.

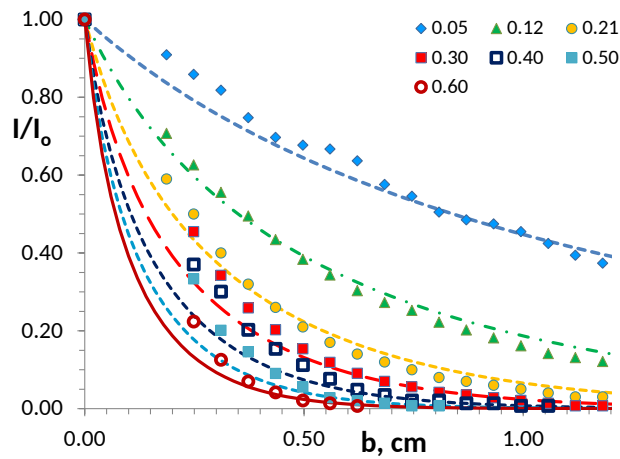
276 For each catalyst the entire dataset (dependence on  $b$  and  $C_{cat}$ ) was fitted with eq. (7) to  
 277 obtain specific coefficient for absorption ( $\epsilon_{abs}$ ) and scattering ( $\epsilon_{sca}$ ), which are related to the  
 278 Kubelka-Munk coefficients  $\kappa$  and  $\sigma$  according to the following equations:

$$279 \quad \epsilon_{abs}(\lambda) = \frac{\kappa(\lambda) 10^3}{\ln(10)C_{cat}} \quad (9a)$$

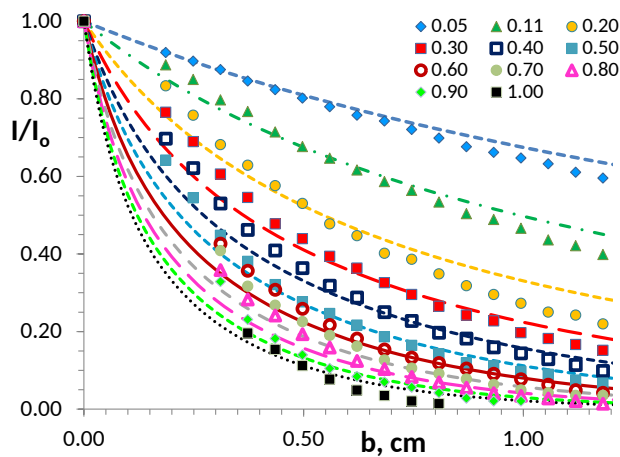
$$280 \quad \epsilon_{sca}(\lambda) = \frac{\sigma(\lambda) 10^3}{\ln(10)C_{cat}} \quad (9b)$$

281

282



283



284 **Figure 3** Normalized radiation intensity  $I / I_0$  as a function at the optical depth  $b$  and catalyst loading  
 285 (in  $\text{g L}^{-1}$ , see legend) for Evonik P25 (top) and Hombikat UV100 (bottom) suspensions. For each catalyst  
 286 the curves were obtained from the best fit of the overall dataset with eq. (7) with  $\epsilon_{abs}$  and  $\epsilon_{sca}$  as the only fit  
 287 parameters for the whole set of catalyst loadings.

288 Figure 3 A,B show the experimental data used to carry out the fit together with the fit  
 289 curves. They described quite well the experimental data. For each catalyst all the data were fit  
 290 with  $\epsilon_{abs}$  and  $\epsilon_{sca}$  as the only fit parameters, considering for each profile the actual catalyst  
 291 loading. Surprisingly, although the simplest approximation for absorption/scattering, the K-M  
 292 equation works quite well, as reported for a variety of other experimental situations. [35]

293 The lamp emission spectrum is narrow and the spectral variations of the optical constants  
 294 could be considered minor. In the case of polychromatic light the approach here proposed can  
 295 still be employed, but the obtained optical constants would have an empirical and average  
 296 meaning only. They allow comparing the properties of different photocatalysts under real  
 297 illumination conditions, but can only partially compared with the values measured with  
 298 monochromatic light.

299 The fit parameters are reported in Table 1 together with the ratio between  $\epsilon_{sca}$  and  $\epsilon_{abs}$ . The  
 300 specific absorption coefficient for TiO<sub>2</sub> P25 is five times larger than that of TiO<sub>2</sub> UV100,  
 301 while the specific scattering coefficient is roughly 2 times larger for TiO<sub>2</sub> P25, as also  
 302 observed in ref. [34]. The ratio between the coefficients is 4 and 9 for P25 and UV100,  
 303 respectively, suggesting that - from an optical point of view - P25 better exploits the incident  
 304 light than UV 100, despite of the higher  $\epsilon_{sca}$ . The larger absorption coefficient potentially  
 305 leads to a larger photocatalytic rate. Conversely, the larger scattering coefficient of P25  
 306 compared to UV100 limits  $\chi$ , which is always lower for P25 than for Hombikat UV100. The  
 307 fraction of light scattered does not contribute to the overall rate and ultimately represents an  
 308 unused contribution.

309

310 **Table 1. Coefficients for scattering  $\epsilon_{sca}$  and absorption  $\epsilon_{abs}$ , and their ratio for TiO<sub>2</sub> specimens Evonik**  
 311 **P25 and Hombikat UV 100.**

	<b>Evonik P25</b>	<b>Hombikat UV100</b>
$\epsilon_{sca}$ , cm <sup>2</sup> g <sup>-1</sup>	(6.5±1.1)·10 <sup>3</sup>	(3.1±0.3)·10 <sup>3</sup>
$\epsilon_{abs}$ , cm <sup>2</sup> g <sup>-1</sup>	(1.6±0.2)·10 <sup>3</sup>	(0.34±0.03)·10 <sup>3</sup>
$\epsilon_{sca}/\epsilon_{abs}$ <b>ratio</b>	4.1±0.9	9.0±1.7

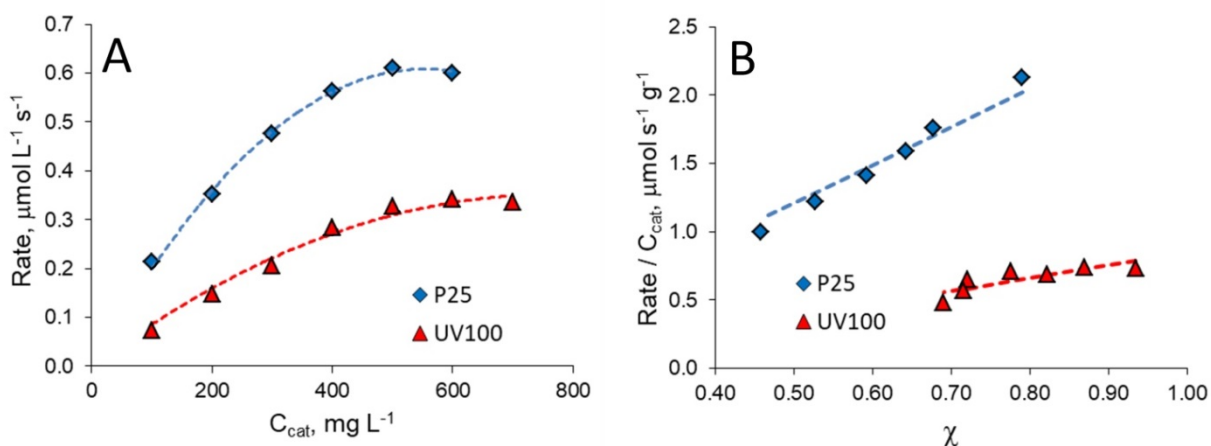
312

313 The data of Table 1, including the  $\epsilon_{sca}$  to  $\epsilon_{abs}$  ratios, are of the same order of magnitude, but  
 314 significantly lower than those previously reported [34], and in particular of figures 6,7 of ref.  
 315 [36]. The reason can be easily related to the different adopted procedures and setup. While in  
 316 ref. [34] the incident light is monochromatic, and therefore the optical parameters are referred  
 317 to a specific wavelength, in this work the parameters obtained are mediated over the range of  
 318 wavelengths emitted by the used lamp, and effectively used in the cell volume. As it occurs  
 319 experimentally, as photons scattered outside the lateral walls do not contribute the

320 photocatalytic process, in the setup here used they are not collected by the detector. Then the  
 321 obtained values refer only to the lamp used, but are relevant for the (commonly) used  
 322 experimental setup. In addition, the method here proposed is easier to apply, because it does  
 323 not require *i*) the use of a spectrophotometer equipped with total diffuse reflectance accessory  
 324 as used by Cabrera *et al.* to evaluate absorption and forward scattering; *ii*) the application of  
 325 the quite complex radiative transport equation to obtain the scattering and absorption  
 326 coefficients. [34] The data reported in Table 1 are more similar to the experimental extinction  
 327 coefficients reported by Egerton [22], obtained on rutile powders with different particle size.  
 328 In agreement with Egerton's data, for the photocatalysts here investigated we found a marked  
 329 decrease in the extinction coefficient with decreasing particle size.

#### 330 4.2. Photodegradation experiments

331 The influence of the optical parameters on the degradation rate was evaluated by carrying  
 332 out formic acid photodegradation experiments in the presence of P25 and UV100 specimens,  
 333 for which the absorption and scattering coefficients were evaluated. Formic acid was chosen  
 334 as substrate because it is not subjected to back-reactions.[37] Furthermore, thanks to the  
 335 extremely reducing potential of the couple  $\text{CO}_2^\bullet/\text{CO}_2$  [38] the formate radical is able to inject  
 336 an electron into the conduction band evolving directly to  $\text{CO}_2$ . This process is usually  
 337 reported as current doubling [39-42]. Firstly, we followed the degradation of 0.2 mM formic  
 338 acid at different concentrations of  $\text{TiO}_2$  suspensions, thus working at significant different  $\chi$   
 339 values. This concentration (0.2 mM) was the lowest concentration for which it was  
 340 experimentally possible to follow the decay profile. At the same time this concentration was  
 341 supposed to be low enough to allow the approximation  $y/2 \ll 2$ , and, therefore, the use of eq.  
 342 (5) to describe the kinetic data.



343

344 **Figure 4. A) HCOOH degradation rates vs.  $C_{\text{cat}}$  and B) degradation rates normalized for  $C_{\text{cat}}$  as a**  
 345 **function of  $\chi$  for  $\text{TiO}_2$  P25 and UV100 at 0.2 mM initial [HCOOH].**

346 The time evolution of formic acid for P25 and UV100 at different  $C_{cat}$  are reported in  
 347 Figure 3-SM. Figure 4A shows the rate as a function of  $C_{cat}$ . The rates normalized for the  
 348 catalyst concentration are reported in Figure 4B as functions of  $\chi$ . The term  $rate_{obs}/C_{cat}$   
 349 proportionally increases with increasing  $\chi$ , as predicted by eq. (5), for both catalysts.

350 The role of factors other than the light scavenging for the two semiconductors was  
 351 estimated by evaluation of  $k'$  in eq. (5) through the fit of the data reported in Figure 4B. In eq.  
 352 (5)  $k'$  is the only fit parameter, being known the other terms under the square root, namely  $I_0$   
 353 and  $\varepsilon_{abs}$ . The nonlinear fit (as  $k'$  is both in the intercept and slope of the straight line) gives the  
 354 cumulative constant  $k'$ , which is reported with its contributions in eq. (10): [15]

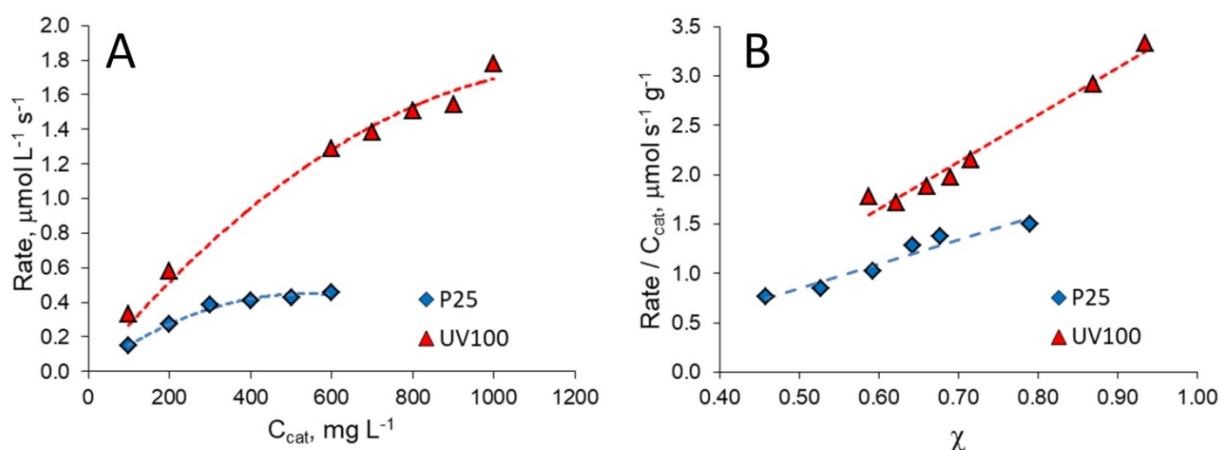
$$355 \quad k' = k_{ox,s}k_{red,s}K_{Red_1}K_{Ox_2}C_{Red_1}[Ox_{2,f}]S(2k_{R,s}a_s^2)^{-1}(1 + K_{Ox_2}[Ox_{2,f}])^{-1} \quad (10)$$

357 where  $k_{ox,s}$  and  $k_{red,s}$  are the rate constants for the oxidation and the reduction processes,  
 358  $K_{Red_1}$  and  $K_{Ox_2}$  are the adsorption constants for substrate and the oxidant (in this case oxygen)  
 359 respectively,  $C_{Red_1}$  is the molar concentration of the substrate in solution,  $[Ox_{2,f}]$  is the molar  
 360 concentration of oxygen in the water bulk,  $S$  is the photocatalyst specific surface area,  $k_{R,s}$  is  
 361 the recombination rate constant between surface-trapped electrons and holes,  $a_s$  is the specific  
 362 area of the exchange site on the photocatalyst surface. The intrinsic (crystallographic phase,  
 363 surface defects, band potentials, doping, ...) and extrinsic properties (pH, composition of the  
 364 solution, presence complexing ions, ...) influence all the kinetic and thermodynamic constants  
 365 included in the parameter  $k'$ .

366 The obtained values for  $k'$  are 0.36 and 0.22  $\mu\text{mol s}^{-1} \text{g}^{-1}$  for Evonik P25 and for Hombikat  
 367 UV100, respectively. Dividing  $k'$  by  $C_{red}$  and  $S$  one gets the value of the kinetic cumulative  
 368 constants independent on the substrate concentration and equal  $k''=3.6 \times 10^{-8}$  and  $1.1 \times 10^{-8} \text{ m s}^{-1}$   
 369  $^1$  for Evonik P25 and UV100, respectively. Then the bundle of constants (kinetic and  
 370 thermodynamic) is about 3 times lower for UV100. The intrinsic heterogeneity of the  $\text{TiO}_2$   
 371 P25 structure (with the contemporary presence of two crystallographic phase, anatase and  
 372 rutile, closely interacting) has been often reported as the driving force able to increase the  
 373 kinetics of separation of the photo-formed charge carriers and consequently decrease the  
 374 recombination kinetics. [43, 44] Eq. (10) shows that  $k''$  is inversely proportional to the  
 375 recombination rate constant. Therefore, supposing similar reaction and partitioning constants  
 376 for P25 and UV100, the lower  $k''$  values for UV100 could be ascribed to a recombination  
 377 process more marked (larger  $k_{R,s}$ ) on this photocatalyst than on  $\text{TiO}_2$  P25.

378 A larger concentration of formic acid (1.0 mM) was also tested at different concentrations  
 379 of  $\text{TiO}_2$  (i.e. at different  $\chi$  values) as done for the lower concentration. The time evolution of  
 380 formic acid for P25 and UV100 at different  $C_{cat}$  are reported in Figure 4-SM. At 1 mM of  
 381 formic acid it can be observed from Figure 5A that: i) UV100 outperformed P25, contrarily to

382 the degradations carried out at low concentration; *ii*) the degradation rate with UV100 was  
 383 significantly higher than at 0.2 mM; and *iii*) P25 displayed nearly the same degradation rate at  
 384 the two formic acid concentrations. Although the rate normalized for  $C_{cat}$  is linear versus  $\chi$   
 385 (Figure 5B), the fit with eq. (5) is inconsistent, because the slope, especially for UV100,  
 386 implies  $\varepsilon_{abs}$  values significantly different from those reported in Table 1. Then at higher  
 387 concentration the approximation on which eq. (5) was derived is no more valid, that is  
 388  $y/2 \ll 2$  is no more legitimate. It is here useful to recall that  $y$  increases with  $C_{red}$ .  
 389 Furthermore, at larger substrate concentration other kinds of surface sites not involved at low  
 390 concentration could be interested, making the kinetic description of the process more  
 391 complex, as previously observed for the photocatalytic transformation of glycerol on TiO<sub>2</sub>  
 392 P25. [19, 21] There it was observed that passing from low to higher concentrations of  
 393 substrate, there is a change of the basic mechanism of electron transfer, from the direct one (at  
 394 the interface), favoured by surface complexation, to an indirect one (across the interface), in  
 395 which the substrate is not bound.[37]



396

397 **Figure 5. A) HCOOH degradation rates vs.  $C_{cat}$  and B) degradation rates normalized for  $C_{cat}$  as a**  
 398 **function of  $\chi$  for TiO<sub>2</sub> P25 and UV100 at 1.0 mM initial [HCOOH].**

## 399 5. Conclusions

400 The rate is influenced by a large variety of parameters that are difficult to evaluate. Under  
 401 defined conditions we proved that optical properties of catalysts can be easily evaluated, and  
 402 that their contribution to the overall efficiency can be assessed through the  $\chi$  parameter. The  
 403 method here proposed can be used to calculate the scattering and absorption properties  
 404 averaged over the emission spectrum of the lamp employed in the photocatalytic reactor.  
 405 Consequently, it is possible to easily uncover the most promising photocatalyst from an  
 406 optical point of view.

407 The degradation rate of formic acid changes accordingly with the eq. (5). Experimental  
 408 data can be properly described by the quadratic kinetic model in the conditions of relatively

409 low quantum yield. [15] Moreover, given the optical parameters, the evaluation of  $k'$  from the  
410  $rate/C_{cat}$  vs  $\chi$  plot allows to assess a lumped parameter specific of each catalyst, reflecting the  
411 base physical processes of charge carriers, catalyst surface area and substrate adsorption  
412 constant. This evaluation is not possible when comparing only the rate, mainly if this is  
413 obtained at a given  $C_{cat}$  in a custom experimental setup. The proposed approach can be the  
414 starting point for fixing conditions to compare different photocatalysts. In particular, besides  
415 the substrate concentration, the catalysts have to be compared to the same  $\chi$  value. This is  
416 important in the growing field of the development of new and more efficient photocatalysts.

## 417 **Acknowledgements**

418 Dedication. The authors dedicate this work to the memory of professor E. Pelizzetti (16  
419 February 1944- 25 July 2017) – University of Torino, Italy - for his pioneering research in  
420 heterogeneous photocatalysis, which inspired many of the papers cited in this work.

421 The financial support from project Ricerca Locale – Torino University – is gratefully  
422 acknowledged.

## 423 **References**

- 424 [1] A.R. Ribeiro, O.C. Nunes, M.F.R. Pereira, A.M.T. Silva, *Environ. Int.* 75 (2015) 33-51.  
425 [2] A. Di Paola, E. García-López, G. Marci, L. Palmisano, *J. Hazard. Mater.* 211-212 (2012)  
426 3-29.  
427 [3] P. Pichat (Ed.), *Photocatalysis: fundamentals, materials and potential*, 1st ed., MDPI,  
428 Basel, Switzerland 2016.  
429 [4] J. Schneider, D. Bahnemann, J. Ye, G.L. Puma, D.D. Dionysiou (Eds.), *Photocatalysis:*  
430 *fundamentals and perspectives*, 1st ed., The Royal Society of Chemistry, Cambridge, UK,  
431 2016.  
432 [5] J.C. Colmenares, Y.-J. Xu (Eds.), *Heterogeneous photocatalysis: from fundamentals to*  
433 *green applications*, 1st ed., Springer-Verlag, Berlin Heidelberg, 2016.  
434 [6] C. McCullagh, N. Skillen, M. Adams, P.K.J. Robertson, *J. Chem. Technol. Biotechnol.* 86  
435 (2011) 1002-1017.  
436 [7] C. Minero, V. Maurino, D. Vione, *Photocatalytic mechanisms and reaction pathways*  
437 *drawn from kinetic and probe molecules*, in: P. Pichat (Ed.) *Photocatalysis and Water*  
438 *Purification*, Wiley-VCH Verlag GmbH & Co. KGaA, Weinheim, 2013, pp. 53-72.  
439 [8] P. Calza, C. Minero, E. Pelizzetti, *Environ. Sci. Technol.* 31 (1997) 2198-2203.  
440 [9] J.-M. Herrmann, *Catal. Today* 53 (1999) 115-129.

- 441 [10] M.A. Henderson, *Surf. Sci. Rep.* 66 (2011) 185-297.
- 442 [11] C. Minero, *Catal. Today* 54 (1999) 205-216.
- 443 [12] J. Cunningham, G. Al-Sayyed, S. Srijaranai, G.R. Helz, Adsorption of model pollutants  
444 onto TiO<sub>2</sub> particles in relation to photoremediation of contaminated water, in: G.R. Helz,  
445 R.G. Zepp, D.G. Crosby (Eds.) *Aquatic and Surface Photochemistry*, Taylor & Francis,  
446 Boca Raton, FL, USA, 1994, pp. 317-348.
- 447 [13] Y. Xu, C.H. Langford, *J. Photochem. Photobiol. A-Chem.* 133 (2000) 67-71.
- 448 [14] A.V. Emeline, V. Ryabchuk, N. Serpone, *J. Photochem. Photobiol. A-Chem.* 133 (2000)  
449 89-97.
- 450 [15] C. Minero, D. Vione, *Appl. Catal. B: Environ.* 67 (2006) 257-269.
- 451 [16] A.V. Emeline, V.K. Ryabchuk, N. Serpone, *J. Phys. Chem. B* 109 (2005) 18515-18521.
- 452 [17] M. Minella, F. Bertaina, C. Minero, *Catal. Today* 315 (2018) 9-18.
- 453 [18] D. Monllor-Satoca, R. Gómez, M. González-Hidalgo, P. Salvador, *Catal. Today* 129  
454 (2007) 247-255.
- 455 [19] V. Maurino, A. Bedini, M. Minella, F. Rubertelli, E. Pelizzetti, C. Minero, *J. Adv. Oxid.*  
456 *Technol.* 11 (2008) 184-192.
- 457 [20] S. Valencia, F. Cataño, L. Rios, G. Restrepo, J. Marín, *Appl. Catal. B: Environ.* 104  
458 (2011) 300-304.
- 459 [21] C. Minero, A. Bedini, V. Maurino, *Appl. Catal. B: Environ.* 128 (2012) 135-143.
- 460 [22] T. Egerton, *Molecules* 19 (2014) 18192.
- 461 [23] F. Pellegrino, L. Pellutiè, F. Sordello, C. Minero, E. Ortel, V.-D. Hodoroba, V.  
462 Maurino, *Appl. Catal. B: Environ.* 216 (2017) 80-87.
- 463 [24] F. Ramiro-Manzano, P. Atienzar, I. Rodriguez, F. Meseguer, H. Garcia, A. Corma,  
464 *Chem. Commun.* (2007) 242-244.
- 465 [25] J.I.L. Chen, G. von Freymann, V. Kitaev, G.A. Ozin, *J. Am. Chem. Soc.* 129 (2007)  
466 1196-1202.
- 467 [26] F. Sordello, C. Duca, V. Maurino, C. Minero, *Chem. Commun.* 47 (2011) 6147-6149.
- 468 [27] G. Camera-Roda, V. Augugliaro, A.G. Cardillo, V. Loddo, L. Palmisano, F. Parrino, F.  
469 Santarelli, *Catal. Today* 259 (2016) 87-96.
- 470 [28] G. Camera-Roda, V. Loddo, L. Palmisano, F. Parrino, *Catal. Today* 281 (2017) 221-230.
- 471 [29] A.K. Alexander, *J. Phys. D* 40 (2007) 2210.
- 472 [30] G. Palmisano, V. Loddo, V. Augugliaro, M. Bellardita, G. Camera Roda, F. Parrino,  
473 *Chem. Eng. J.* 262 (2015) 490-498.
- 474 [31] R.J. Brandi, M.A. Citroni, O.M. Alfano, A.E. Cassano, *Chem. Eng. Sci.* 58 (2003) 979-  
475 985.



- 476 [32] K. Mehrotra, G.S. Yablonsky, A.K. Ray, *Chemosphere* 60 (2005) 1427-1436.
- 477 [33] M. Minella, M. Demontis, M. Sarro, F. Sordello, P. Calza, C. Minero, *J. Mater. Sci.* 50  
478 (2015) 2399-2409.
- 479 [34] M.I. Cabrera, O.M. Alfano, A.E. Cassano, *J. Phys. Chem.* 100 (1996) 20043-20050.
- 480 [35] P.S. Mudgett, L.W. Richards, *Appl. Opt.* 10 (1971) 1485-1502.
- 481 [36] M.L. Satuf, R.J. Brandi, A.E. Cassano, O.M. Alfano, *Ind. Eng. Chem. Res.* 44 (2005)  
482 6643-6649.
- 483 [37] J.F. Montoya, J.A. Velásquez, P. Salvador, *Appl. Catal. B: Environ.* 88 (2009) 50-58.
- 484 [38] W.H. Koppenol, J.D. Rush, *J. Phys. Chem.* 91 (1987) 4429-4430.
- 485 [39] T.L. Villarreal, R. Gómez, M. González, P. Salvador, *J. Phys. Chem. B* 108 (2004)  
486 20278-20290.
- 487 [40] I. Mora-Seró, T.L. Villarreal, J. Bisquert, Á. Pitarch, R. Gómez, P. Salvador, *J. Phys.*  
488 *Chem. B* 109 (2005) 3371-3380.
- 489 [41] N. Hykaway, W.M. Sears, H. Morisaki, S.R. Morrison, *J. Phys. Chem.* 90 (1986) 6663-  
490 6667.
- 491 [42] S.R. Morrison, *Electrochemistry at semiconductor and oxidized metal electrodes*, Plenum  
492 Press 1980.
- 493 [43] T. Ohno, K. Sarukawa, K. Tokieda, M. Matsumura, *J. Catal.* 203 (2001) 82-86.
- 494 [44] R.I. Bickley, T. Gonzalez-Carreno, J.S. Lees, L. Palmisano, R.J.D. Tilley, *J. Solid State*  
495 *Chem.* 92 (1991) 178-190.